Supporting Information for “The role of lattice dynamics in ferroelectric switching”

Section 1: Phase Field Coefficients

Parameter	Value	Unit
α_1	$4*10^5*(T-1193)$	$J*m^4/C^2$
α_{11}	$3*10^8$	$J*m^8/C^4$
α_{12}	$1.188*10^8$	$J*m^8/C^4$
β_1	$6*10^6*(T-1198)$	J/rad^2
β_{11}	$3.44*10^{10}$	J/rad^4
β_{12}	$6.799*10^{10}$	J/rad^4
λ_{11}	0.288	$1/rad^2$
λ_{12}	-0.097	$1/rad^2$
λ_{44}	0.206	$1/rad^2$
t_{11}	$4.532*10^9$	$J*m^4/(C^2*rad^2)$
t_{12}	$2.266*10^9$	$J*m^4/(C^2*rad^2)$
t_{44}	$-4.84*10^9$	$J*m^4/(C^2*rad^2)$
C_{11}	$2.95*10^{11}$	GPa
C_{12}	$1.18*10^{11}$	GPa
C_{44}	$0.74*10^{11}$	GPa
Q_{11}	0.0603	m^4/C^2
Q_{12}	-0.0111	m^4/C^2
Q_{44}	0.0176	m^4/C^2

Section 2: Note on Calculating in-plane and out-of-plane components of elastic strain

Since the elastic strain is the total strain minus the eigenstrain, the total strain should be equal to the eigenstrain of the original state $\lambda_{ijkl}\theta_k^{ref}\theta_l^{ref} + Q_{ijkl}p_k^{ref}p_l^{ref}$ $(i,j = 1,2)$, where the superscript "ref" denotes the original state before the switching process. Thus the in-plane elastic strain during switching is $\lambda_{ijkl}\theta_k\theta_l + Q_{ijkl}p_kp_l$-$\lambda_{ijkl}\theta_k^{ref}\theta_l^{ref} + Q_{ijkl}p_k^{ref}p_l^{ref}$ $(i,j = 1,2)$. From the traction free surface conditions, $\sigma_{13} = \sigma_{23} = \sigma_{33} = 0$, we can calculate the out-of-plane components of the elastic strain.

Figure S1. Growth, transfer, and characterization of freestanding BFO membranes. a, Schematic of the SRO/BFO/SRO/LSMO/STO heterostructure growth, freestanding membrane release and transfer. b, AFM images of the BFO film (a) and freestanding membrane (b) with thickness of 35nm. The roughness is 223 pm and 406 pm, respectively.

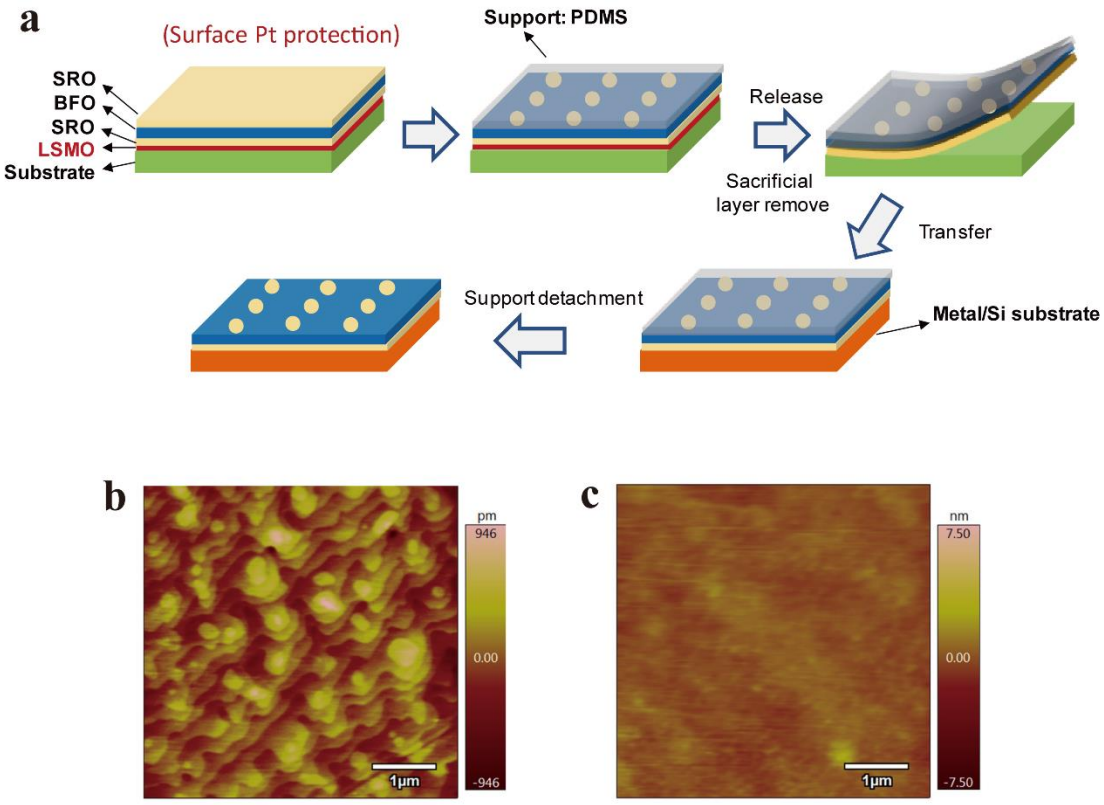

Figure S2. XRD pattern and Reciprocal space maps (RSM) of BFO samples before and after freestanding. a, 2θ-ω XRD patterns of the BFO/SRO/LSMO with BFO thickness of 35 nm before and after lift off. **b, c,** RSM of the sample (b) before and (c) after lift off. **d, e, f,**RSM of the samples after lift off with BFO thickness of 8, 60 and 100 nm, respectively.

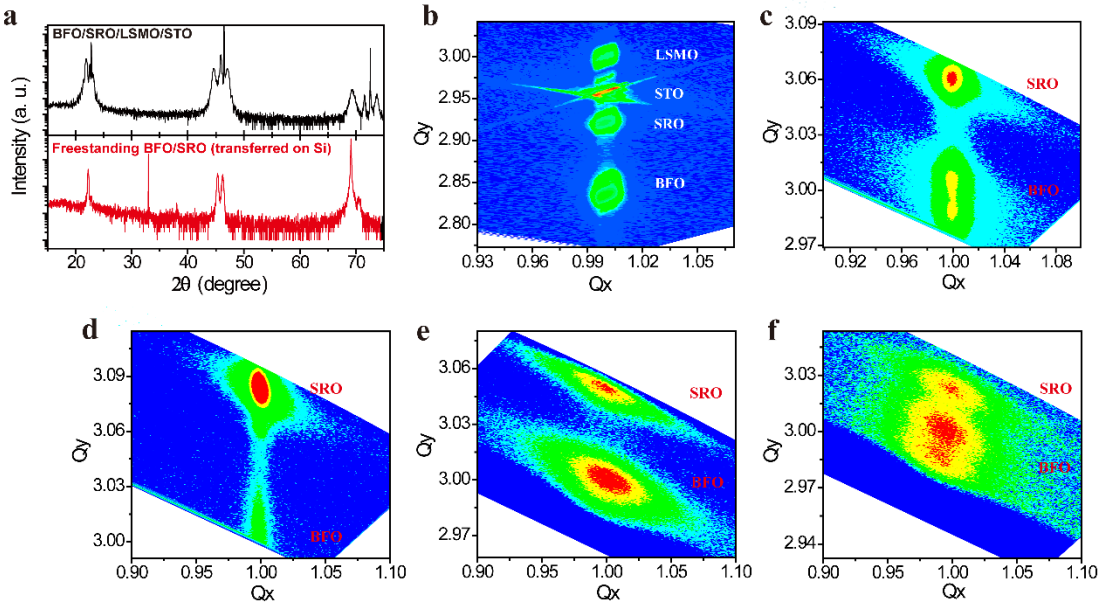

Figure S3. Domain patterns of the 100-nm BFO film and free-standing membrane. a, b, out-plane PFM amplitude images of film (a) and free-standing membrane (b). **c, d**, in-plane PFM phase images of film (c) and free-standing membrane (d). **e, f**, out-plane PFM phase images of film (e) and free-standing membrane (f). The free-standing membrane features larger domain size and an exclusively 180° domain pattern.

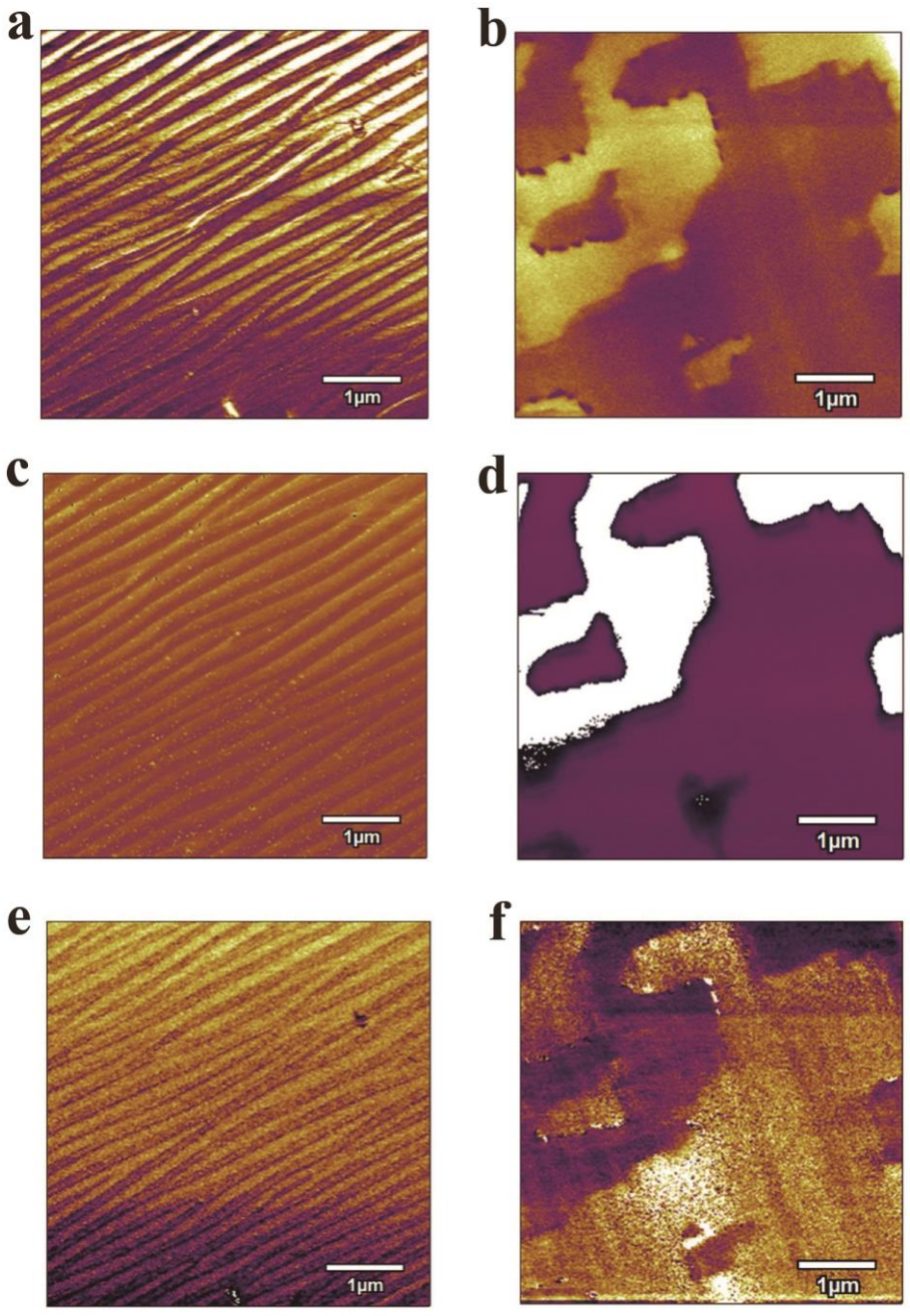

Figure S4. Domain patterns of the BFO films and free-standing membranes with different thicknesses. a, d, in-plane PFM amplitude images of BFO film (a) and free-standing membrane (b) with thickness of 60 nm. **b, e**, in-plane PFM amplitude images of BFO film (b) and free-standing membrane (e) with thickness of 20 nm. **c, f**, in-plane PFM amplitude image of BFO film (c) and free-standing membrane (f) with thickness of 8 nm. All the free-standing membranes feature larger size of domain and the emergence of an exclusively 180° domain pattern.

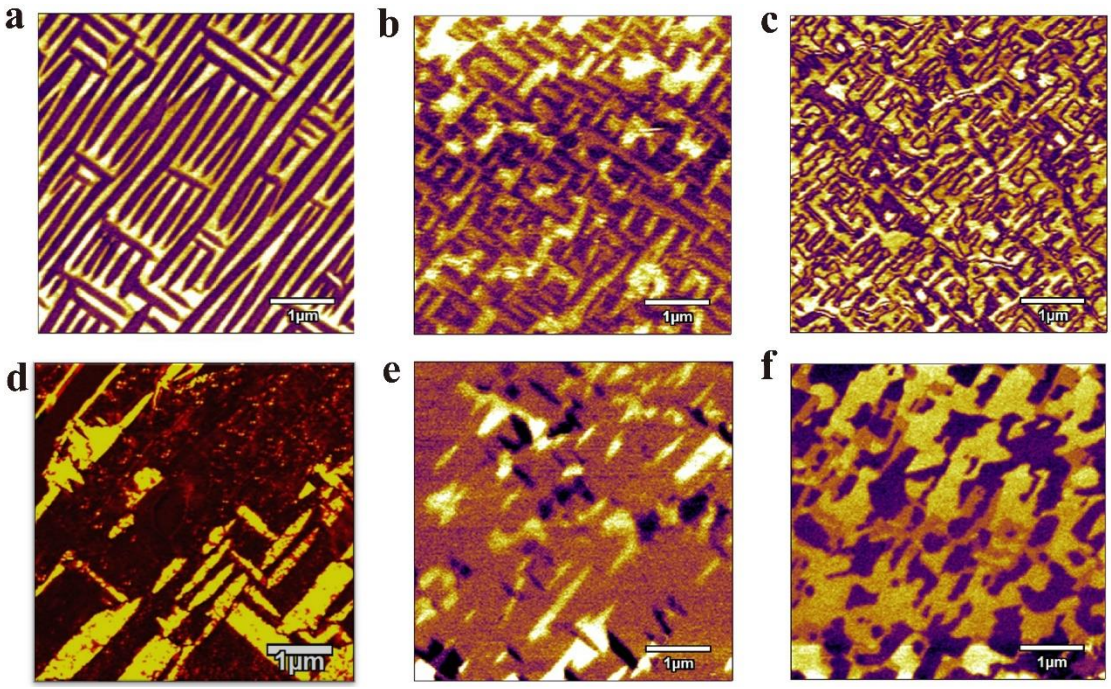

Figure S5. Phase-field simulation of a BFO layer before and after lift-off, with 2-variant initial domain structure. Domain structure of a BFO film with a 2-variant domain walls, before (**a., b.**) and after (**c., d.**) removal lift-off the substrate.

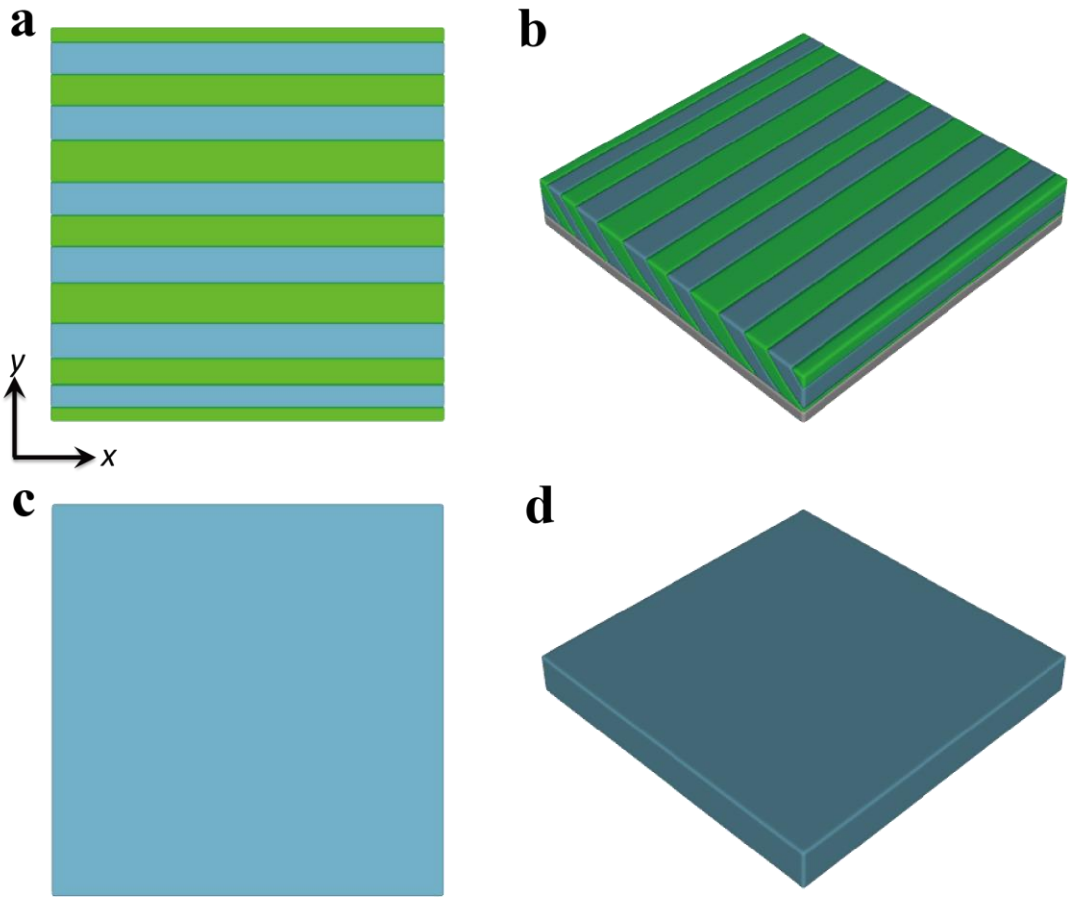

Figure S6. Ferroelectric polarization versus electric voltage (P-V loops) of the BFO films and transferred free-standing membranes. a, b, P-V loops of the SRO/BFO/SRO capacitors for a 100-nm BFO (a) before and (b) after lift off. The measurements were carried out across a wide frequency range from 1 Hz to 100 kHz. **c, d,** P-V loops of the SRO/BFO/SRO capacitors with 35-nm BFO (c) before and (d) after lift off. The measurements were carried out across a wide frequency range from 50 Hz to 100 kHz, at temperature of 100 K.

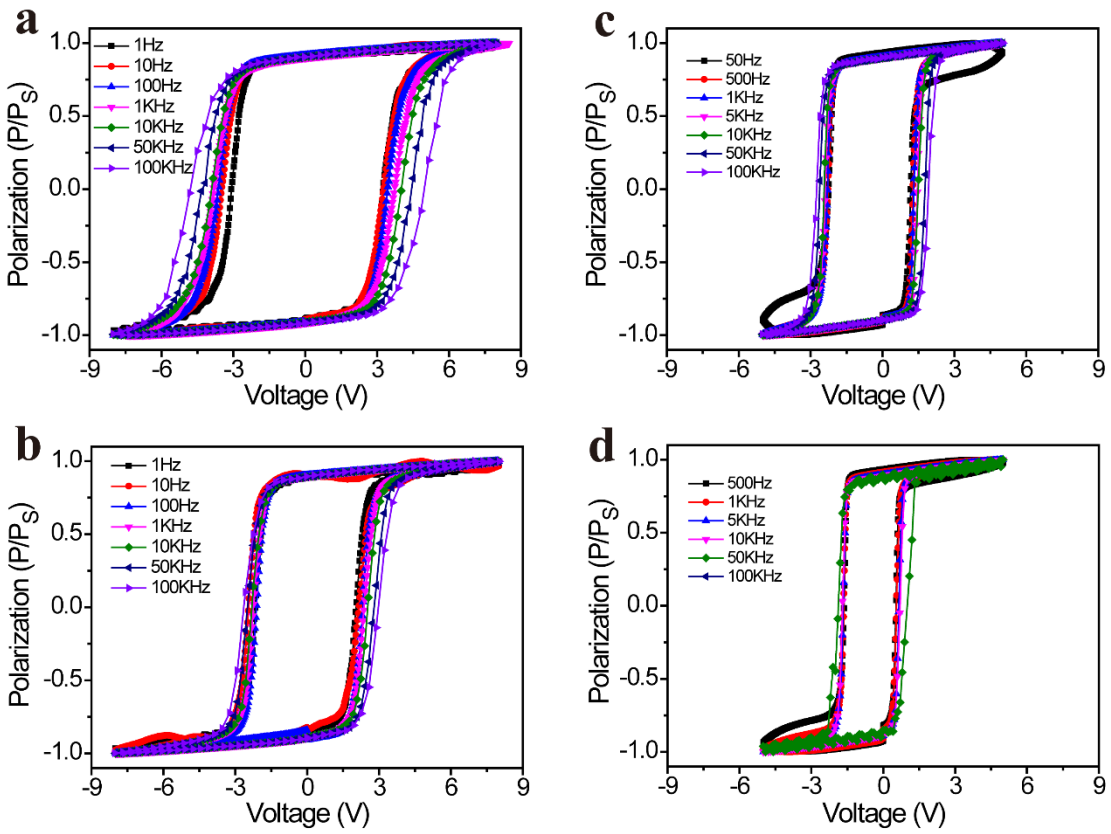

Figure S7. Frequency dispersion of measured Vc. Measured coercive voltage for various excitation frequencies. Fits are discussed in **Table S1.**

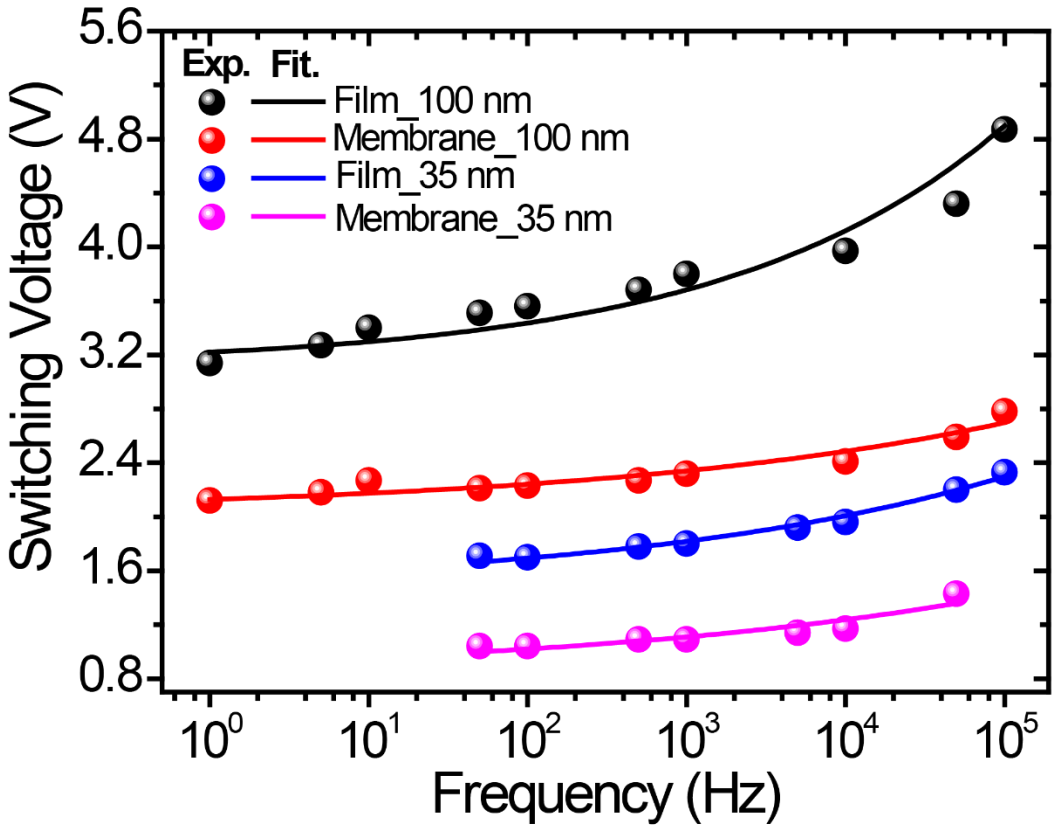

Figure S8. Piezoelectric Phase and Amplitude response of the BFO samples with varied thickness before and after lift off. a, d, 100 nm. **b, e,** 60 nm, **c, f,** 35 nm. We can see obvious decrease of switching voltage after lift off.

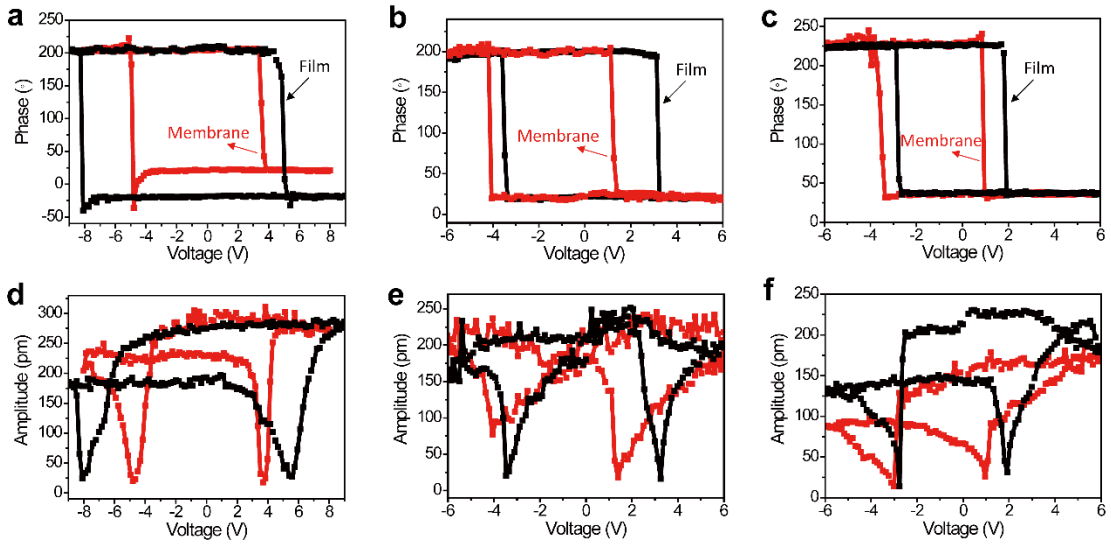

Figure S9. Switching dynamics in the SRO/BFO/SRO capacitors samples before and after lift off. a, b, The switching current responses for the samples with BFO thickness of 25 nm, before and after lift off, respectively.

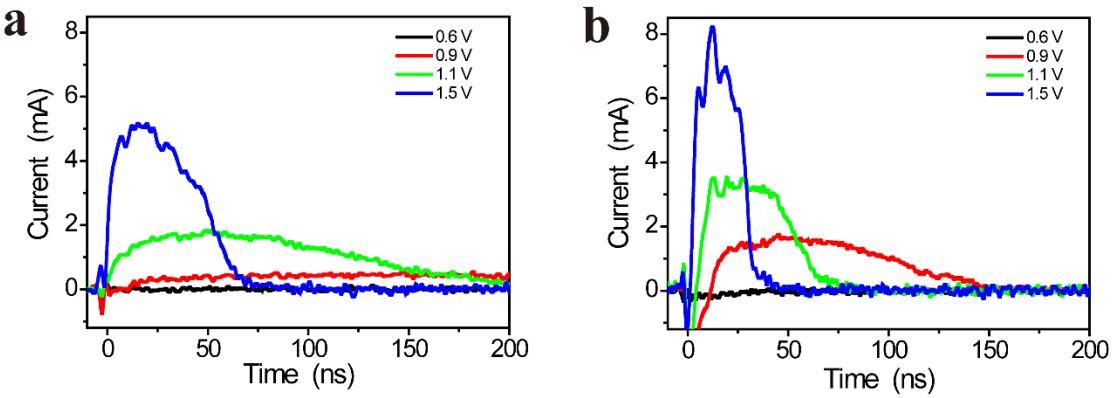

Figure S10. Clamped vs. Membrane Switching Energy Landscapes for BTO and PTO. a. and **b.** show calculated switching energy landscapes for prototypical ferroelectrics BTO and PTO, respectively, showing energy barrier height reductions of ~30% in BTO and ~35% in PTO. Calculations are performed by clamping non-switching order parameters.

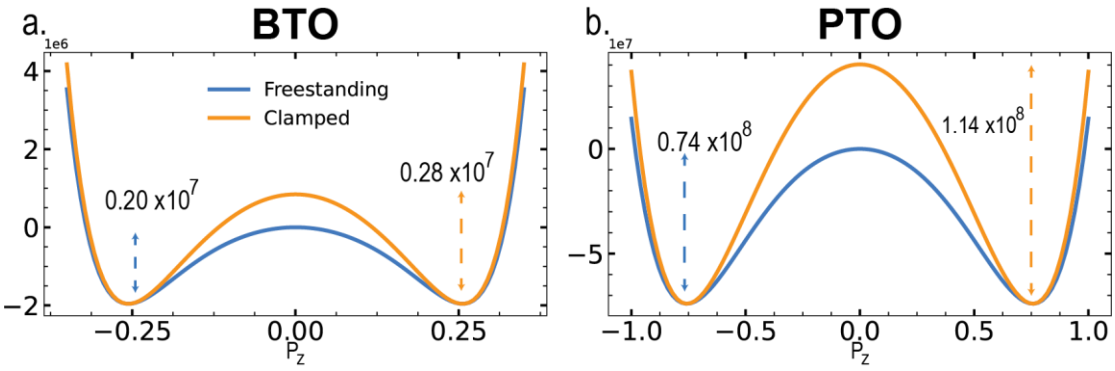

Figure S11. Free energy evolution during the switching process under an externally applied voltage for clamped film and membrane cases without oxygen octahedral tilts. Horizontal axis is the time in picosecond (ps) and vertical axis is the average energy of the corresponding component within the whole simulation system in J cm^{-3}. **(a)** Elastic energy. **(b)** Electrostatic energy. **(c)** Landau energy. **(d)** Total free energy which is the summation of the elastic electrostatic, and Landau energy.

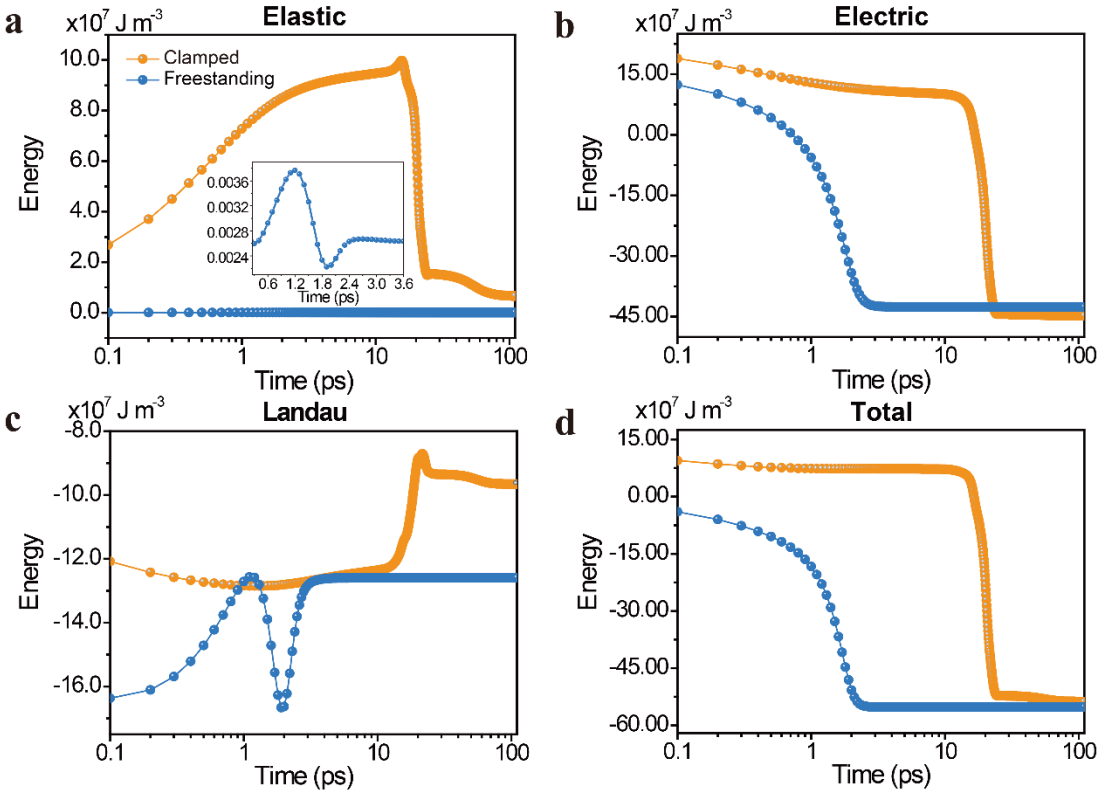

Table S1. "Static" switching voltage, $V_{c,0}$, and the frequency dispersion exponent, b, obtained from the fitting using the Ishibashi model[1]

Sample	$V_{c,0}$ (V)	b
BFO clamped film 100nm	3.12	0.25
BFO membrane 100nm	2.03	0.16
BFO clamped film 35nm	1.46	0.18
BFO membrane 35nm	0.81	0.15

Observed coercivity in ferroelectric hysteresis loop measurements is known to vary with the applied voltage frequency as $V_c = V_{c,0} + a\, f^b$, [1,2] where $V_{c,0}$ is the thermodynamic limit of switching voltage (i.e., "Static" switching voltage, at zero frequency), f is the testing frequency, and a and b are obtained by fitting the frequency dependent data. The so-called "frequency dispersion" can be evaluated through the exponent b. As shown in **Fig. S7**, the data for all the samples fits well to this model, with fitting parameters shown (**Table S1**). In addition to the large reduction of static switching voltage estimated by the $V_{c,0}$, for each thickness when going from a clamped film to a membrane, it also interesting that the frequency dispersion of the freestanding membranes have both lower b values (indicating less dispersive behavior) and also less variability between thicknesses than their clamped film counterparts (clamped films vary from 0.25 at 100 nm to 0.18 at 25 nm, while the freestanding membranes vary only from 0.16 to 0.15 for the same thickness variation).

References

1. Ishibashi, Y. *et al.* A theory of D-E hysteresis loop. *Integr. Ferroelectr.***9**, 57-61 (1995).

2. Liu, L. *et al.* Frequency-dependent decoupling of domain-wall motion and lattice strain in bismuth ferrite. *Nat. Commun.***9**, 4928 (2018).